Journal of Applied Physics

RESEARCH ARTICLE | MARCH 09 2026

Cut-enabled anisotropic and non-reciprocal elasticity in chiral metamaterials

Hao Jin ; Changyou Peng ; Xiao Yang ; Shichao Niu ; Ning An

J. Appl. Phys. 139, 103102 (2026)
https://doi.org/10.1063/5.0321385

Journal of Applied Physics ARTICLE pubs.aip.org/aip/jap

Cut-enabled anisotropic and non-reciprocal elasticity in chiral metamaterials

Cite as: J. Appl. Phys. **139**, 103102 (2026); doi: 10.1063/5.0321385
Submitted: 7 January 2026 · Accepted: 20 February 2026 ·
Published Online: 9 March 2026

View Online Export Citation CrossMark

Hao Jin,[1] Changyou Peng,[1] Xiao Yang,[1,a)] Shichao Niu,[2] and Ning An[3,4,a)]

AFFILIATIONS

[1]School of Mechanical Engineering, Hangzhou Dianzi University, Hangzhou 310018, China
[2]Key Laboratory of Bionic Engineering, Ministry of Education, Jilin University, Changchun 130022, China
[3]Key Laboratory of Advanced Spatial Mechanism and Intelligent Spacecraft, Ministry of Education, School of Aeronautics and Astronautics, Sichuan University, Chengdu 610065, China
[4]Department of Civil, Environmental and Mechanical Engineering, University of Trento, Trento 38123, Italy

[a)]**Authors to whom correspondence should be addressed:** yangxiao0431@foxmail.com and anning@scu.edu.cn

ABSTRACT

We introduce strategically placed cuts into chiral mechanical metamaterials to achieve strongly anisotropic and static non-reciprocal elasticity in a fully passive architecture. Under loading, the cuts switch between open states that preserve auxetic kinematics and closed contact states that trigger an abrupt stiffness increase, thereby breaking symmetry. By systematically varying the cut topology—the number, placement, and orientation of cuts—we identify regimes with sharp stiffness transitions and pronounced uniaxial and orthogonal non-reciprocity. A topological coding strategy is proposed to program these responses at the unit-cell level. These results establish cut-mediated opening and contact as a general mechanism for designing non-reciprocal mechanical metamaterials.

I. INTRODUCTION

Mechanical metamaterials exploit geometry to realize effective properties beyond those of conventional solids, including negative Poisson's ratio, strong anisotropy, and programmable stiffness.[1] Of particular interest is the achievement of directional and non-reciprocal elastic responses in passive structures, which could enable static functionalities such as mechanical diodes,[2] adaptive load-bearing,[3] as well as dynamic applications in vibration isolation and wave manipulation.[4,5] In linear, conservative systems, however, reciprocity and symmetry impose strong constraints,[6] and existing approaches to break them often rely on active elements, temporal modulation, or complex multi-material designs.

Chiral mechanical metamaterials constitute a classical and well-studied class of architected lattices. Their rotational kinematics give rise to intrinsic auxetic behavior, and their geometry–property relations have been extensively investigated, making them a canonical platform for exploring architected elasticity.[7] Despite their rich kinematics, the elastic response of conventional chiral lattices remains largely reciprocal and symmetry governed, offering limited capability for programming directional asymmetry or non-reciprocal behavior through geometry alone.

Recent studies have suggested that chiral geometries may host asymmetric coupling associated with mechanical activity.[7] Similar principles of chirality and symmetry breaking are also actively explored in other wave-based metamaterial domains to achieve exotic physical phenomena, such as chiral bound states in the continuum in plasmonic metasurfaces.[8] While active matter and spatiotemporal modulation readily break reciprocity,[9] realizing such behavior in passive solids requires strong deformation-dependent nonlinearities. Self-contact has enabled extreme auxetic responses,[10,11] and cut-induced contact has recently been proposed to generate multimodal non-reciprocity.[12,13] This behavior is distinct from the violation of Maxwell–Betti reciprocity in linear elasticity,[2,9] as non-reciprocity does not occur within the linear elastic and small-deformation regime. Instead, the cuts drive the structure into distinct contact configurations under tension vs compression, resulting in different tangent stiffnesses. Consequently, the observed phenomenon is fundamentally a path-dependent, geometrically nonlinear effective non-reciprocity. However, a general geometric strategy for programming anisotropy and static non-reciprocity in passive architected solids is still lacking.

Here, we show that strategically introducing cuts into conventional chiral metamaterials provides a simple and passive route to overcome these limitations. Under mechanical loading, the cuts allow deformation-dependent transitions between open states, which preserve the intrinsic auxetic kinematics of the chiral architecture, and closed contact states, which trigger discontinuous changes in stiffness symmetry and effective elasticity. By systematically varying the number, orientation, and topology of cuts, we demonstrate strongly anisotropic and non-reciprocal elastic responses and identify regimes with abrupt stiffness transitions and directional asymmetry. These results establish cut-mediated opening and contact as a general mechanism for programming anisotropy and non-reciprocity in mechanical metamaterials.

II. STATIC NON-RECIPROCITY IN CHIRAL METAMATERIAL WITH CUTS

In Fig. 1, we compare a conventional chiral metamaterial with our fourfold cut-mediated design to elucidate the role of cuts in tailoring the mechanical response. The effective behavior is characterized by representative volume element (RVE)[14] analyses, whose accuracy is validated in the end of the paper against experiments and finite-size simulations.

For the conventional chiral metamaterial, the RVE exhibits a negative Poisson's ratio (NPR) under compression due to bending-dominated deformation and cooperative rotation of the chiral units, whereas under tension ligament stretching suppresses rotation, leading to a positive Poisson's ratio (PPR) [see Figs. 1(a1)–1(a2)]. In contrast, the fourfold cut-mediated metamaterial shows an NPR under both tension and compression. Under tension, all cuts open, releasing geometric constraints and enabling an auxetic unfolding mode. Under compression, the cuts aligned with the loading direction open to accommodate rotation, while the transverse cuts progressively close and come into contact, introducing directional constraints [see Figs. 1(b1)–1(b2)].

The corresponding stress–strain responses and Poisson's ratios are shown in Figs. 1(a3), 1(b3), 1(a4), and 1(b4). The conventional design displays nearly symmetric tensile and compressive responses, reflecting a reversible, bending-dominated mechanism without contact. By contrast, the cut-mediated architecture is symmetric only at small strains (up to about 3%), when all cuts remain open and deformation is rotation-dominated. Beyond this regime, contact between transverse cuts under compression redirects load paths into a stretching-dominated state, producing a sharp increase in stiffness and a pronounced asymmetry between tension and compression.

This contact-mediated kinematic transition also governs the evolution of Poisson's ratio. While the conventional metamaterial transitions from a PPR at small strains to an NPR at larger compressive strains due to enhanced unit rotation, the cut-mediated metamaterial exhibits an NPR already at small strains owing to unconstrained auxetic kinematics. Upon contact activation in compression, the growing transverse constraint progressively suppresses lateral expansion, driving Poisson's ratio from negative to positive values.

To quantify the resulting static non-reciprocity, we extract the effective stiffness matrix C_{ij} from the RVE response. The uniaxial non-reciprocity is measured by

$$r_s = \frac{C_{11}^t}{C_{11}^c} \tag{1}$$

(and analogously C_{22}^t/C_{22}^c), capturing the contrast between tensile and compressive stiffness along the same axis. Orthogonal non-reciprocity is defined as

$$r_o = \frac{C_{21}}{C_{12}}, \tag{2}$$

reflecting asymmetry in coupling between orthogonal directions. Unlike classical Maxwell–Betti reciprocity which dictates stiffness tensor symmetry ($C_{ij} = C_{ji}$), the metrics defined here quantify nonlinear, state-dependent effects. Specifically, r compares the instantaneous stiffness C across distinct kinematic states (tension vs compression) driven by contact switching.

Owing to geometric symmetry, both designs remain orthogonally reciprocal, with $r_o \approx 1$ over the entire strain range [see Figs. 1(a5) and 1(b5)]. In contrast, their uniaxial responses differ markedly. The conventional metamaterial maintains $r_s \approx 1$, consistent with similar bending-dominated mechanisms in tension and compression. The fourfold cut-mediated metamaterial exhibits $r_s \approx 1$ only at small strains, but once contact is activated under compression, r_s increases rapidly and saturates, revealing a contact-induced switch from a compliant to a stiff regime and the emergence of strong static non-reciprocity.

III. RESULTS AND DISCUSSIONS

To systematically explore the design space, we adopt a combinatorial strategy encoded by the states of the four ligaments in the RVE. As shown in the left panel of Fig. 2, the ligaments are indexed clockwise from the top left (1–4). Each ligament is assigned a ternary state—solid, type-1 cut, or type-2 cut—leading to coding sequences with four digits, such as 0000 or 1012. By filtering configurations that preserve structural connectivity, we obtain a set of 15 topological designs that constitute a programmable library of mechanical units.

The responses of these configurations can be classified into four distinct elastic categories, labeled as (a) through (d) in the right panel of Fig. 2. In each sub-figure, the deformation maps are color-coded where green regions indicate NPR ($\nu < 0$) and beige regions indicate PPR ($\nu > 0$). The layout within each panel reveals specific reciprocity characteristics: the top row compares orthogonal reciprocity under compression (1 vs 2), while the bottom row compares orthogonal reciprocity under tension. Vertically, the first column contrasts uniaxial reciprocity along the two-direction, and the second column contrasts uniaxial reciprocity along the one-direction.

The first category, illustrated in Fig. 2(a), is represented by the pristine 0000 design. In the compressive phase, the structure exhibits symmetric deformation shaded in green with $C_{12}^c = C_{21}^c$. Conversely, the tensile phase is shaded in beige, signifying a transition to PPR behavior. This confirms orthogonal reciprocity with $r_o = 1$, but the sign inversion of Poisson's ratio from compression to tension highlights strong uniaxial non-reciprocity where $r_s \neq 1$.

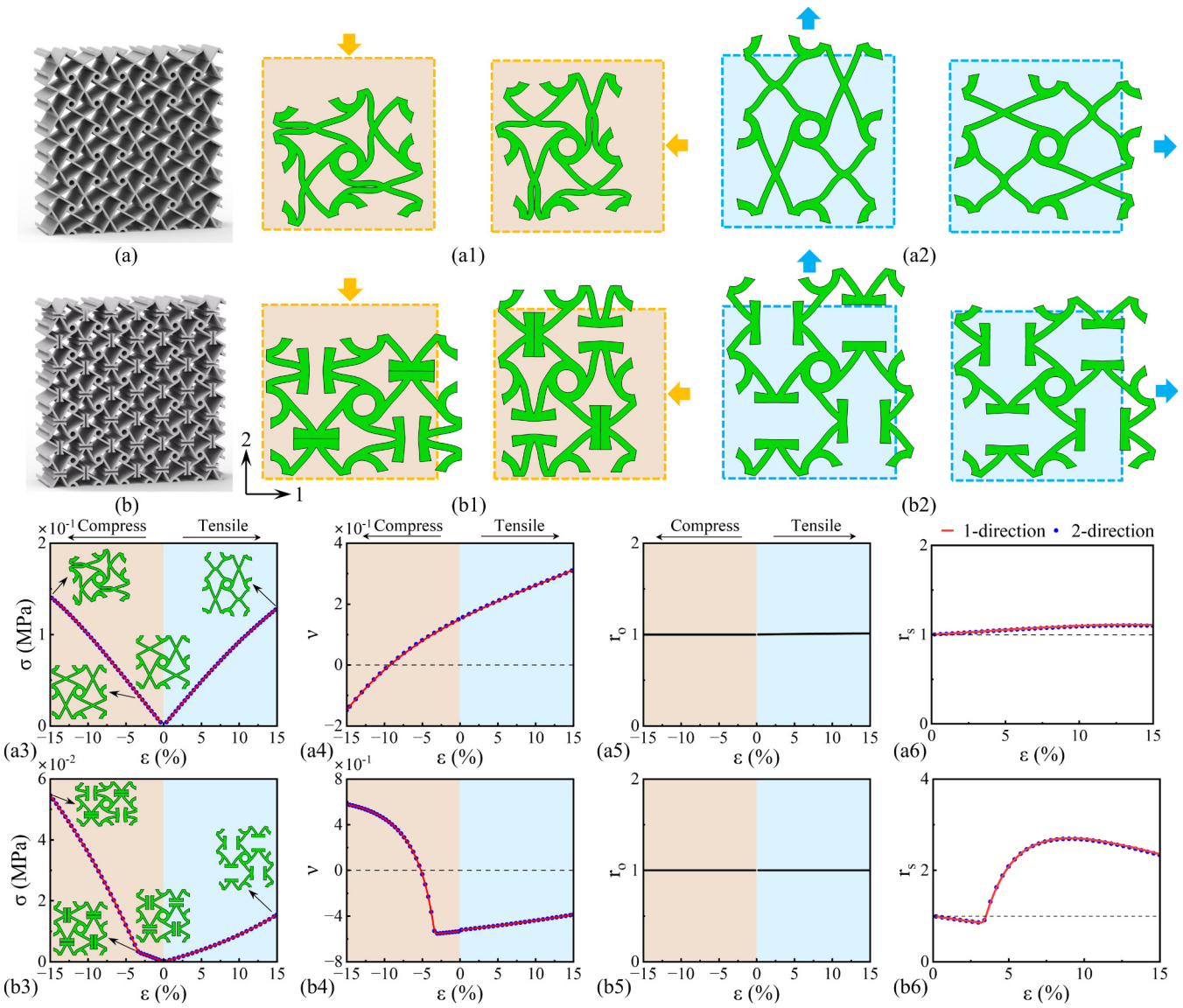

FIG. 1. Cut-induced transition in elastic behavior of chiral metamaterials. (a) Baseline anti-chiral metamaterial exhibiting nearly isotropic stiffness and reciprocal response. (b) Cut-enabled chiral metamaterial with fourfold-symmetric cuts. The introduction of cuts fundamentally modifies the macroscopic elastic response: under compression, the cuts close and engage in contact (contact state), whereas under tension, they remain open (separated state). This cut-mediated transition leads to pronounced changes in stiffness and deformation modes, producing strong uniaxial non-reciprocity ($r_s \neq 1$) while preserving orthogonal reciprocity ($r_o = 1$). Panels (a1)–(a2) and (b1)–(b2) illustrate representative deformation modes under compressive and tensile loading, respectively. Panels (a3)–(a6) and (b3)–(b6) show the corresponding stress–strain responses, Poisson's ratio, and reciprocity metrics in the one- and two-directions.

The second category, shown in Fig. 2(b), includes designs like the symmetric 1111 configuration. These structures share the same orthogonal reciprocity where $r_o = 1$ and isotropy as the first category but display a reversed kinematic switch. Here, compression induces contact-driven expansion shown in beige, while tension activates the rotational opening mechanism leading to contraction shown in green.

Finally, the categories in Figs. 2(c) and 2(d) emerge from hybrid cut patterns such as 1012. In these cases, the structural asymmetry breaks the balance of the stiffness matrix. Unlike the switching behaviors in isotropic designs, these anisotropic configurations exhibit persistent polarity. As evidenced by the uniform coloration, category (c) maintains positive expansion (beige) under both tension and compression, whereas category (d) remains

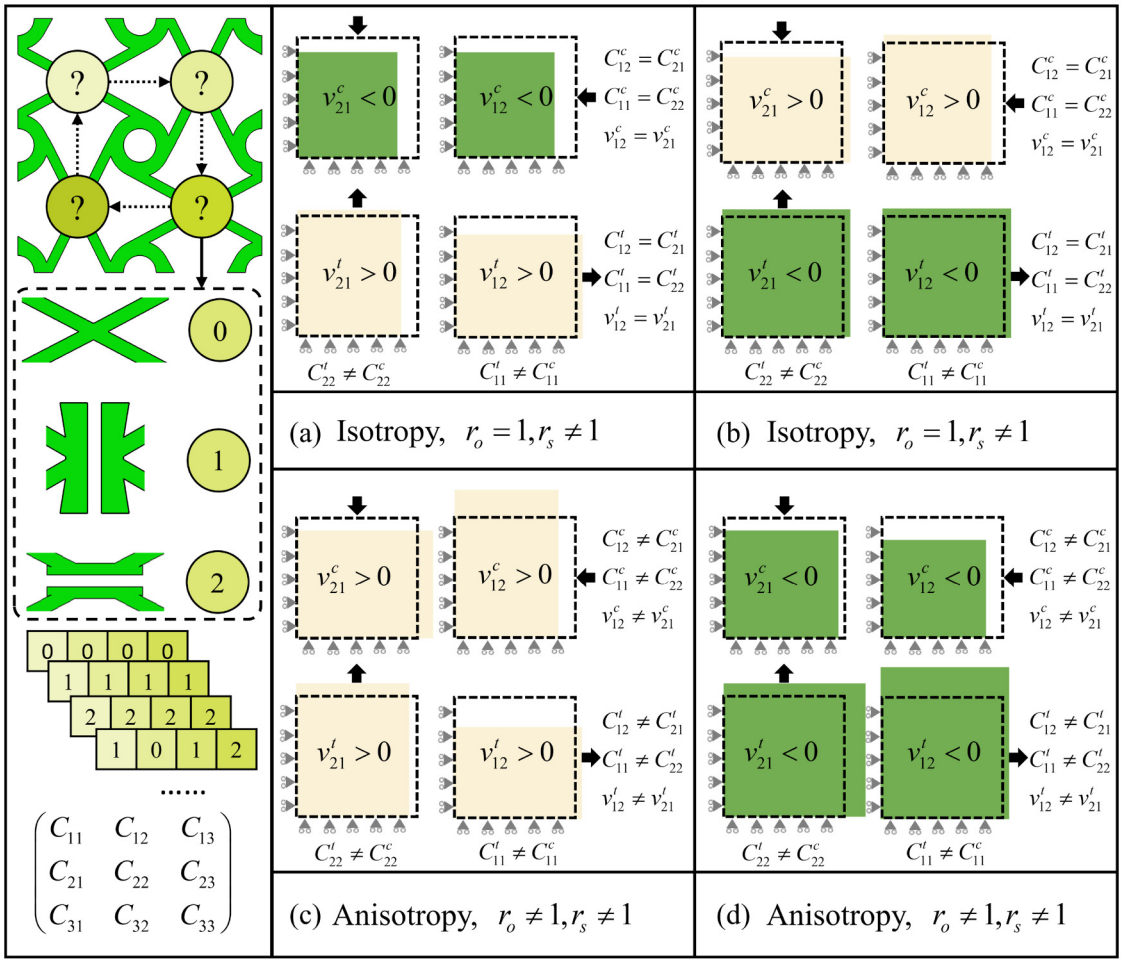

FIG. 2. Topological coding strategy and classification of non-reciprocal mechanical responses. (Left) Topological coding applied to the four ligaments of the RVE, where states 0, 1, and 2 represent the pristine ligament and two distinct cut orientations, respectively. This coding generates a library of configurations with programmable uniaxial and orthogonal non-reciprocity. (Right) Classification of the resulting architectures into four categories based on stiffness matrix symmetry and deformation modes. Panels (a)–(d) schematically illustrate the deformation under compression (top row) and tension (bottom row), where dashed outlines indicate the initial shape and colors denote the sign of Poisson's ratio (green: negative; beige: positive). Categories (a) and (b) preserve orthogonal reciprocity ($r_o = 1$) but exhibit uniaxial non-reciprocity ($r_s \neq 1$). In contrast, categories (c) and (d) display broken symmetry in the orthogonal stiffness terms and anisotropy, resulting in orthogonal non-reciprocity ($r_o \neq 1$) and uniaxial non-reciprocity ($r_s \neq 1$).

strictly auxetic (green). Despite this stability in Poisson's ratio sign, these designs exhibit orthogonal non-reciprocity where $C_{12} \neq C_{21}$ and $r_o \neq 1$, effectively combining direction-dependent stiffness with the violation of Maxwell–Betti reciprocity. It should be noted that isotropy and anisotropy in this paper specifically refer to the equivalence of mechanical properties (such as stiffness and non-reciprocity ratio) along the two orthogonal principal axes (one-direction and two-direction), which is governed by the symmetry of the unit cell.

To demonstrate the versatility of the proposed strategy, we selected three representative cases from the topological library for detailed analysis in Fig. 3; the remaining configurations are provided in the supplementary material.

The first design (code 2222) retains the geometric symmetry of the baseline structure (code 0000). Consequently, the stress–strain and Poisson's ratio curves under one- and two-loading coincide completely, preserving strict orthogonal reciprocity ($r_o = 1$). However, this uniform type-2 cut configuration exhibits a unique performance limit: it achieves the maximum isotropic uniaxial non-reciprocity (r_s) among all 15 identified designs. This indicates that optimizing cut topology alone can significantly amplify the stiffness contrast between tensile and compressive states without compromising orthogonal symmetry.

The second design (code 1220) embodies the complex mechanical behavior of the low-symmetry regime. The stress–strain curves reveal multiple distinct turning points. These features are

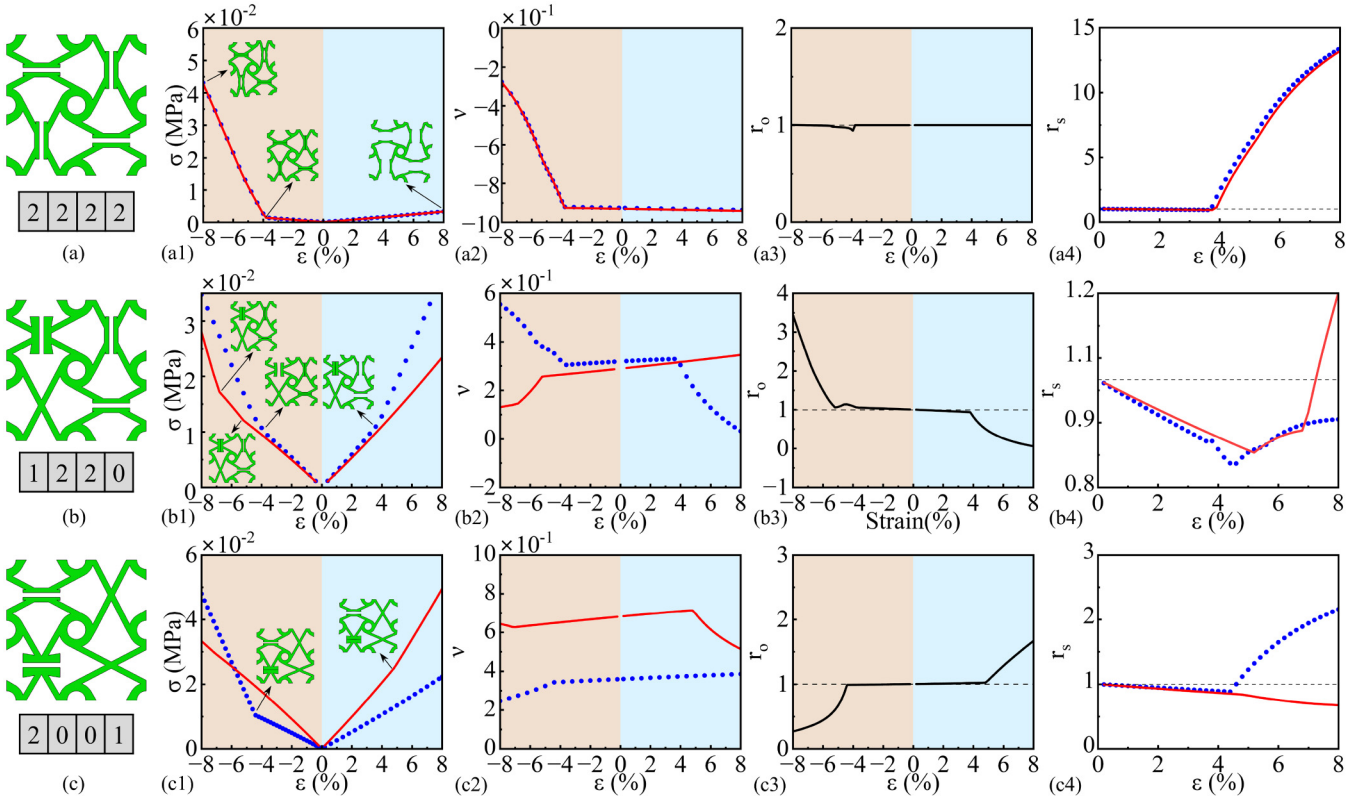

FIG. 3. Representative programmable mechanical responses of cut-embedded chiral metamaterials corresponding to topological codes (a) 2222, (b) 1220, and (c) 2001. Subplots with indices 1–4 display the evolution of stress (σ), Poisson's ratio (ν), orthogonal non-reciprocity (r_o), and uniaxial non-reciprocity (r_s) vs strain (ε). Red solid and blue dotted lines denote the one- and two-directions, while orange and blue backgrounds indicate compression and tension. (a) Code 2222 achieves the maximum isotropic r_s while maintaining strict orthogonal reciprocity. (b) Code 1220 exhibits multiple turning points due to multi-stage contact, demonstrating significant orthogonal non-reciprocity ($r_o \neq 1$). (c) Code 2001 displays similar $r_o \neq 1$ but is distinguished by decoupled anisotropic behavior with diverging r_s trends.

attributed to the stepwise closing of cut interfaces, where contacts occur asynchronously as strain increases. This multi-stage mechanism drives the bifurcation of Poisson's ratio trends, where ν_{12} and ν_{21} evolve in distinct paths, resulting in strong orthogonal non-reciprocity ($r_o \neq 1$) that varies significantly with strain.

The third design (code 2001) highlights programmable directional control. While this configuration exhibits orthogonal non-reciprocity ($r_o \neq 1$) similar to that of code 1220, it is distinguished by its decoupled anisotropic behavior. Specifically, the uniaxial non-reciprocity ratios (r_s) for the one- and two-directions display diverging evolution trends: one direction exhibits a hardening-dominated non-reciprocity ($r_s > 1$) while the other shows a softening or suppressed trend. This confirms that specific cut combinations can effectively decouple the non-reciprocal responses along orthogonal axes.

Figure 4 provides a comprehensive atlas of the mechanical performance for all 15 topological configurations. By mapping the normalized maximum non-reciprocity indices within the 8% strain limit alongside the stiffness and Poisson's ratio at 8% strain, the figure quantifies the breadth of the programmable property space.

As shown in Fig. 4(a), the distribution of this non-reciprocal capacity is governed by the crystallographic symmetry of the unit cell, consistent with Neumann's principle, which states that the symmetry of the physical property tensors must include the symmetry elements of the crystal point group.[7,11] The uniform fourfold cut design (code 2222) belongs to the C_4 point group. The invariance of the effective stiffness tensor $\mathbf{C}$ under the 90° rotation operator ($R_{z,\pi/2}$) imposes strict constraints on the off diagonal components, enforcing $C_{11} = C_{22}$ and restricting the difference between C_{12} and C_{21}.[7] Consequently, the high symmetry of code 2222 acts as a gatekeeper, preserving orthogonal reciprocity ($r_o \approx 1$) throughout the deformation. In contrast, asymmetric coding patterns(code 1010) break this rotational symmetry,[11] reducing the system to a lower symmetry group (e.g., C_2 or triclinic C_1). This symmetry breaking releases the constraints on the off diagonal terms of the constitutive tensor, allowing contact nonlinearity to manifest as a significant inequality between C_{12} and C_{21}, thereby leading to the pronounced orthogonal non-reciprocity ($r_o \neq 1$) observed in these designs.

The stiffness moduli at 8% strain shown in Fig. 4(b) confirm the feasibility of directional decoupling. The topology strategy

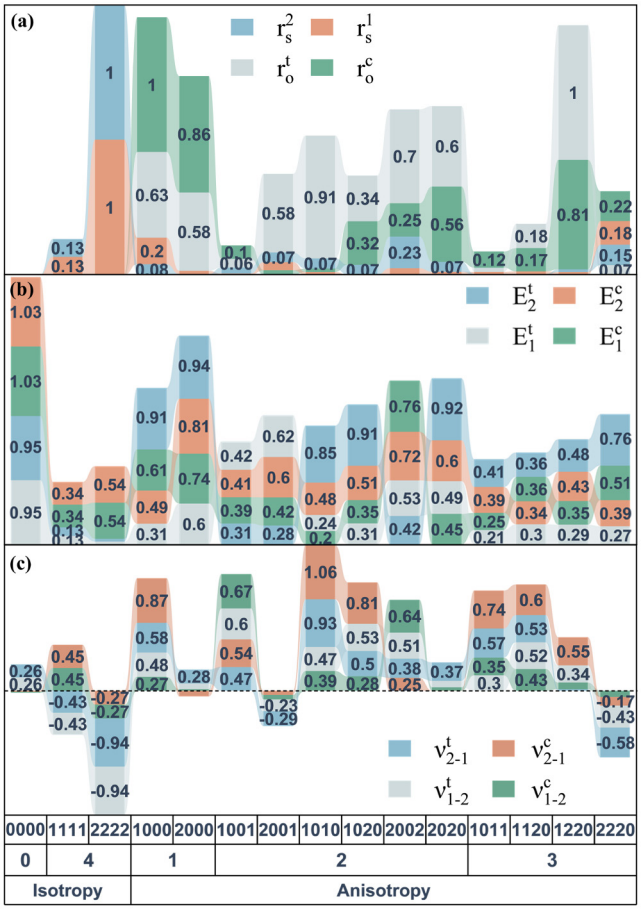

FIG. 4. Quantitative performance library of the 15 topological configurations categorized by symmetry and cut number 0–4. (a) Normalized non-reciprocity indices defined as the maximum absolute deviation from unity $|r - 1|$ within the 8% strain limit. (b) Stiffness moduli E at 8% strain. (c) Poisson's ratio ν values at 8% strain illustrating the wide range of behaviors spanning from auxetic to positive expansion.

allows for independent control over the soft and hard principal axes. A prime example is code 1010 which demonstrates extreme stiffness anisotropy, as its tensile modulus along the two-direction is approximately 3.6 times greater than that of the one-direction. This disparity confirms that specific cut sequences can create materials with strictly directional load-bearing capabilities, breaking the correlation between orthogonal stiffnesses typically found in continuous media.

Finally, Fig. 4(c) maps the distribution of Poisson's ratio values to provide insight into the internal deformation mechanisms governing macroscopic response. The data distinguish between two programmable kinematic modes defined as polarity switching and polarity biasing. In code 2220, the sign of the difference between orthogonal Poisson's ratios reverses completely between tension and compression, indicating a fundamental reconfiguration of the contact mechanism depending on the load direction. Conversely, code 2002 exhibits stable polarity biasing where the difference remains positive in both tension and compression states. This proves that cut topology can deterministically program the behavioral patterns of the non-reciprocal response by selecting between state-dependent flipping and persistent asymmetry.

Our topological coding strategy translates fundamental non-reciprocity into tangible engineering functionalities. The realized uniaxial stiffness asymmetry offers a passive control mechanism for soft robotic actuators, allowing compliance for shape adaptation while ensuring high load capacity for propulsion.[11,12,15] This directional response extends to orthogonal non-reciprocity, which functions as a mechanical diode to enable mechanical logic operations in electronics-free systems.[12] Additionally, the unidirectional deformation amplification observed during the auxetic-to-contact transition is ideal for energy harvesting, where amplified local strains drive piezoelectric elements efficiently under specific loads while providing intrinsic overload protection.[10]

To validate the reliability of the theoretical analysis presented in this study, we conducted a systematic experimental verification of the RVE numerical model accuracy. All experimental specimens were fabricated using Selective Laser Sintering (SLS) additive manufacturing with Thermoplastic Polyurethane (TPU) powder. As shown in Fig. 5, three categories of samples were prepared: (1) standard dog-bone specimens for baseline material characterization, in accordance with ISO 37:2017 standards; (2) full-scale tensile specimens of the chiral metamaterial; and (3) full-scale compressive specimens.

Given the large deformation and nonlinear characteristics of the TPU material, uniaxial tensile tests were performed on the dog-bone specimens. Based on the experimental data, a nearly incompressible second-order Ogden hyperelastic model was employed to describe the constitutive behavior. The fitted material parameters are $\mu_1 = -17.5$, $\mu_2 = 6.53$, $\alpha_1 = 6.53$, and $\alpha_2 = -12.55$. To validate this constitutive model, a 3D finite element model was constructed in Abaqus/Standard using C3D8H elements. The simulation, conducted at a loading rate of 100 mm/min, exhibited excellent agreement with experimental measurements [Fig. 5(c)], confirming that the fitted parameters accurately capture the mechanical response.

Following material calibration, two distinct finite element models were established in Abaqus 2020: an overall model representing the finite-size experimental sample (4×4 array) and an RVE model representing an infinite periodic array (highlighted in red in Fig. 5). Both models were simplified as plane stress problems and discretized using CPS3 elements. Mesh convergence studies were performed (RVE: 18 810 elements and Overall: 485 494 elements). The simulations utilized a general static analysis step with geometric nonlinearity enabled (Nlgeom = On), and Periodic Boundary Conditions (PBCs) were applied to the RVE model. The friction coefficient between cut surfaces was set to 0.47.

The models were subjected to 20% tensile and compressive strains and compared with experimental results. The overall simulation showed high agreement with the experimental response. The RVE simulation aligned with the experimental trends but exhibited a slight numerical deviation. This discrepancy arises from the fundamental difference between the infinite periodic assumption of the RVE and the finite-size boundary effects in experimental

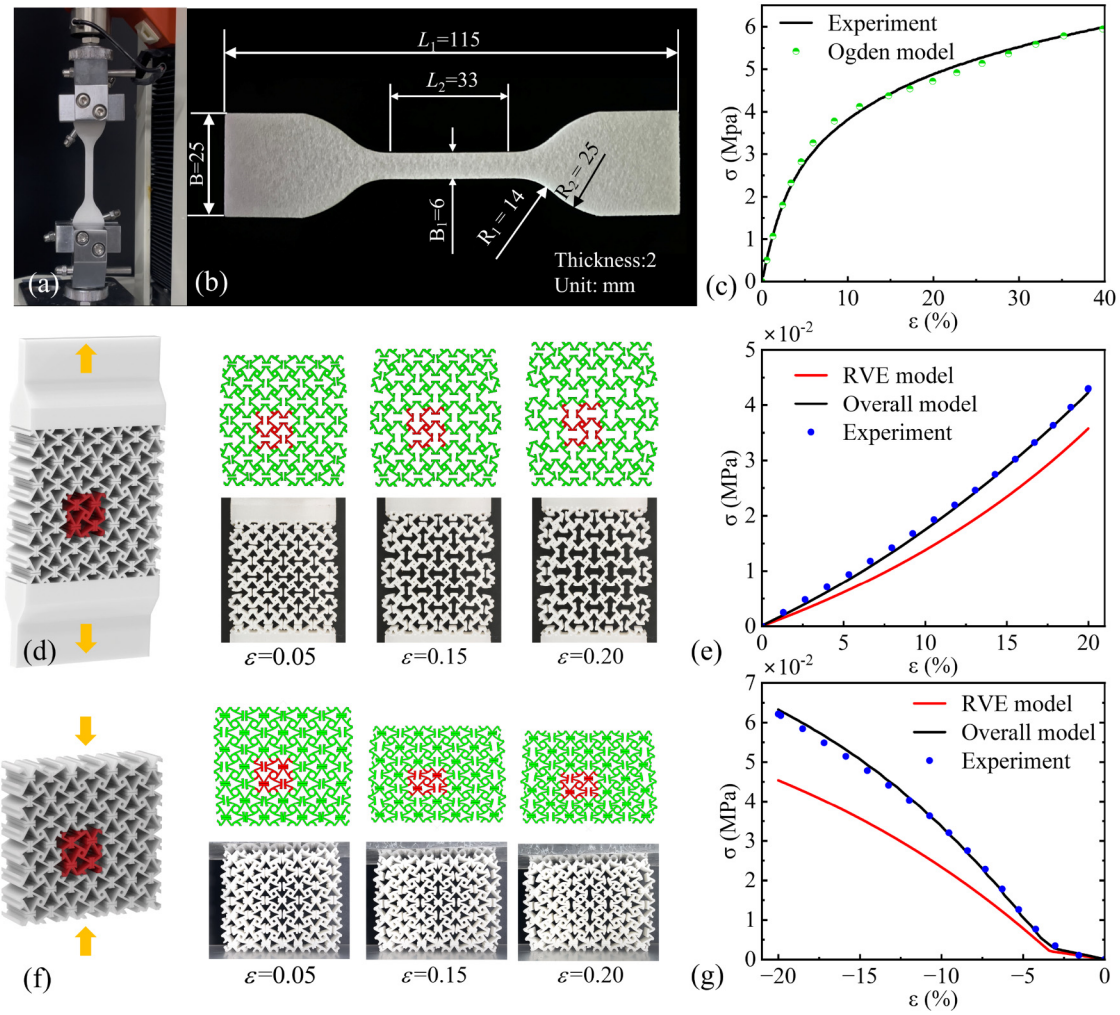

FIG. 5. Material characterization and model validation. (a)–(c) Uniaxial tensile testing of the TPU base material and validation of the second-order Ogden constitutive model. (d)–(g) Comparison of deformation modes and mechanical responses between experiments and FE simulations (Overall and RVE models) under 20% tension [(d)–(e)] and compression [(f)–(g)], verifying the accuracy of the numerical strategy.

samples—an error that diminishes as the number of array units increases. Consequently, the RVE model is confirmed to be a reliable and accurate tool for predicting the anisotropic and non-reciprocal elasticity of the proposed metamaterials.

IV. CONCLUSION

In summary, we have established a deterministic framework for programming anisotropic and non-reciprocal elasticity by embedding cut-induced contact mechanisms into chiral metamaterials. Our systematic exploration of the topological design space uncovers a fundamental physical law stating that the macroscopic non-reciprocal response is strictly governed by the conservation and redistribution of contact-induced nonlinearity modulated by geometric symmetry. We demonstrate that geometric symmetry serves as the primary determinant for the non-reciprocal capacity of the system to enable a precise decoupling of mechanical properties. Preserving structural symmetry concentrates the non-linear potential along the principal axes and allows isotropic designs such as code 2222 to maximize the dynamic range of uniaxial stiffness amplification (r_s) while rigorously suppressing transverse interaction coupling. Conversely, symmetry breaking is identified as the prerequisite for redistributing this capacity into orthogonal modes to unlock significant orthogonal non-reciprocity (r_o) and realize the independent programming of principal stiffness moduli. Crucially, the identified kinematic bifurcations which manifest as polarity switching or stable biasing in Poisson's ratio values provide physical evidence that the cut topology effectively encodes distinct

logic states into the deformation pathway of the material to act as a tunable mechanical switch.

While this study focuses on topological configurations, the geometric parameters offer further dimensions for expanding the physical landscape. Future investigations should address the influence of cut width which dictates the kinematic threshold for contact activation and ligament slenderness which governs the sensitivity to local buckling instabilities. The interaction between cut-induced contact and buckling modes may induce higher-order non-linearities and richer physical phenomena. Moving beyond the unit-cell level, these distinct topological configurations can serve as fundamental building blocks for macroscopic systems. By employing stochastic filling, functionally graded distributions, or advanced inverse design algorithms including topology optimization and generative or diffusion-based machine learning models, it becomes feasible to construct complex meta-structures with tailored macroscopic responses. Such strategies hold immense potential for maximizing directional performance in applications ranging from direction-dependent energy absorption and vibration isolation to intelligent load-bearing systems.

SUPPLEMENTARY MATERIAL

See the supplementary material for the geometric parameters of the RVE and the detailed mechanical characterization of the remaining topological configurations not discussed in the main text.

ACKNOWLEDGMENTS

This work was supported by the National Natural Science Foundation of China (NSFC) (Grant Nos. 52275284, W2521055, 12202295, and W2421002); the Fundamental Research Funds for the Provincial Universities of Zhejiang (Grant No. GK259909299001-008); the Sichuan Science and Technology Program (Grant No. 2025ZNSFSC0845); the Open Project Program of the Key Laboratory for Cross-Scale Micro and Nano Manufacturing, Ministry of Education, Changchun University of Science and Technology (Grant No. CMNM-KF202406); the Opening Project of the Key Laboratory of Bionic Engineering (Ministry of Education), Jilin University (Grant No. K202403); and the Opening Project of the Jiangxi Key Laboratory for Innovative Configuration Aircraft Design, Nanchang, China (Grant No. EI202580427). Ning An also acknowledges support from the China Scholarship Council (No. 202506240177).

AUTHOR DECLARATIONS

Conflict of Interest

The authors have no conflicts to disclose.

Author Contributions

Hao Jin: Formal analysis (equal); Funding acquisition (equal); Investigation (equal); Methodology (equal); Writing – original draft (equal); Writing – review & editing (equal). **Changyou Peng:** Data curation (equal); Formal analysis (equal); Investigation (equal). **Xiao Yang:** Investigation (equal); Supervision (equal); Writing – review & editing (equal). **Shichao Niu:** Project administration (equal); Supervision (equal); Validation (equal). **Ning An:** Conceptualization (equal); Funding acquisition (equal); Writing – review & editing (equal).

DATA AVAILABILITY

The data that support the findings of this study are available from the corresponding authors upon reasonable request.

REFERENCES

[1]K. Bertoldi, V. Vitelli, J. Christensen, and M. Van Hecke, "Flexible mechanical metamaterials," Nat. Rev. Mater. **2**, 1–11 (2017).
[2]C. Coulais, D. Sounas, and A. Alu, "Static non-reciprocity in mechanical metamaterials," Nature **542**, 461–464 (2017).
[3]X. Yao, Z. Meng, A. Wang, Y. Wang, and N. Hu, "Self-locking multistable metamaterials with programmable mechanical properties and static non-reciprocity," Adv. Funct. Mater. e07732 (published online 2025).
[4]J. Veenstra, O. Gamayun, X. Guo, A. Sarvi, C. V. Meinersen, and C. Coulais, "Non-reciprocal topological solitons in active metamaterials," Nature **627**, 528–533 (2024).
[5]L. Wang, J. A. I. Martínez, G. Ulliac, B. Wang, V. Laude, and M. Kadic, "Non-reciprocal and non-Newtonian mechanical metamaterials," Nat. Commun. **14**, 4778 (2023).
[6]M. Shaat, M. Moubarez, M. Khan, M. Khan, and A. Alzo'Ubi, "Metamaterials with giant and tailorable nonreciprocal elastic moduli," Phys. Rev. Appl. **14**, 014005 (2020).
[7]M. Shaat and H. S. Park, "Chiral nonreciprocal elasticity and mechanical activity," J. Mech. Phys. Solids **171**, 105163 (2023).
[8]Y. Tang, Y. Liang, J. Yao, M. K. Chen, S. Lin, Z. Wang, J. Zhang, X. G. Huang, C. Yu, and D. P. Tsai, "Chiral bound states in the continuum in plasmonic metasurfaces," Laser Photonics Rev. **17**, 2200597 (2023).
[9]M. Brandenbourger, X. Locsin, E. Lerner, and C. Coulais, "Non-reciprocal robotic metamaterials," Nat. Commun. **10**, 4608 (2019).
[10]A. Tang, Q. Yang, and J. Liu, "Self-contacting metamaterials achieving asymmetric, non-reciprocal, and adjustable Poisson's ratios that break thermodynamic limits," Compos. Struct. **348**, 118486 (2024).
[11]J. Zhang, M. Xiao, L. Gao, A. Alù, and F. Wang, "Self-bridging metamaterials surpassing the theoretical limit of Poisson's ratios," Nat. Commun. **14**, 4041 (2023).
[12]J. Zhang, S. Zhang, X. Zhou, Y. He, F. Wang, D. Yu, Y. Jiang, M. Xiao, and X. Fang, "Cut-enabled mechanical metamaterials for multimodal and reprogrammable static nonreciprocity," Adv. Sci. **12**, e03455 (2025).
[13]A. Montazeri, M. Rahimi, and H. S. Park, "Non-reciprocity and asymmetric elasticity in twisting chiral metamaterials," Int. J. Mech. Sci. **287**, 109990 (2025).
[14]S. L. Omairey, P. D. Dunning, and S. Sriramula, "Development of an ABAQUS plugin tool for periodic RVE homogenisation," Eng. Comput. **35**, 567–577 (2019).
[15]N. Celi, D. Gong, J. Cai, T. Tang, Y. Xu, and D. Zhang, "Algaesperm: Microalgae-based soft magnetic microrobots for targeted tumor treatment," Small **21**, 2407585 (2025).